Polarization of out-of-plane optical scatter from SiO_2 films grown on photolithographically-generated microrough silicon

Thomas A. Germer[a] and Bradley W. Scheer[b]

[a]*Optical Technology Division, NIST, Gaithersburg, MD 20899*
[b]*VLSI Standards, Inc., 3087 N. First St., San Jose, CA 95134*

ABSTRACT

Bidirectional ellipsometry results are presented for scatter from SiO_2 films grown on photolithographically produced microrough silicon surfaces. The principle direction of the polarization and the degree of linear polarization for scatter directions out of the plane of incidence are compared to results of theoretical modeling for interfacial microroughness in the presence of dielectric layers. The results indicate that light scattered from these surfaces does not behave like that from two truly random rough correlated interfaces. Possible reasons for the lack of agreement between the model and the data are discussed.

Keywords: bidirectional ellipsometry, dielectric films, microroughness, polarimetry, scatter, surfaces

1. INTRODUCTION

Light scattering is often employed to detect roughness, defects, and contaminants on nominally smooth surfaces. The angular distribution of the intensity, quantified by the bidirectional reflectance distribution function (BRDF), can be an indication of the source of the scatter, but is often ambiguous. Recent measurements have demonstrated that the polarization of scattered light is strongly dependent upon the nature of its source. When light is directed onto a surface at an oblique angle with the electric field linearly polarized in the plane of incidence, light scattered into directions away from the specular direction has a polarization which is a signature of the scattering mechanism.[1–3]

The measurement of the polarization of light scattering from rough interfaces is also interesting from the standpoint of the capability of increasing the detection sensitivity to defects in the presence of small amounts of roughness. It was found in previous work that light scattered by microroughness has a high degree of polarization in all scattering directions. This finding enables one to develop microroughness-blind instrumentation simply by placing polarizers into the detection scheme, aligned to only allow light to be detected that is polarized orthogonal to that which would arise from microroughness.[4] If the material under test has dielectric layers, then the polarization of the topographically-induced scatter will change. However, the light from rough interfaces should still remain polarized if the dielectric layers are correlated, and will only exhibit randomness in the polarization (depolarization) if the interfaces are not correlated. Knowledge of the polarization characteristics of light scattering from dielectric layers will enable manufacturers to optimize the design of their defect detection instruments for inspecting materials with dielectric layers. For example, learning about the angular dependence of the depolarization will allow them to avoid using microroughness-blind detection schemes in directions where a large degree of depolarization is expected.

In a previous paper, one of the authors presented models for polarized light scattering from roughness and defects in the presence of dielectric layers.[5] These models demonstrated the feasibility of using polarized light scattering to distinguish between microroughness and defects in a single layer, and to determine the degree of correlation between the two rough interfaces. In this paper, we present experimental results to test the model

Part of the SPIE Conference on Scattering and Surface Roughness II
San Diego, California • July 1998
SPIE Vol. 3426 • 0277-786X/98/$10.00

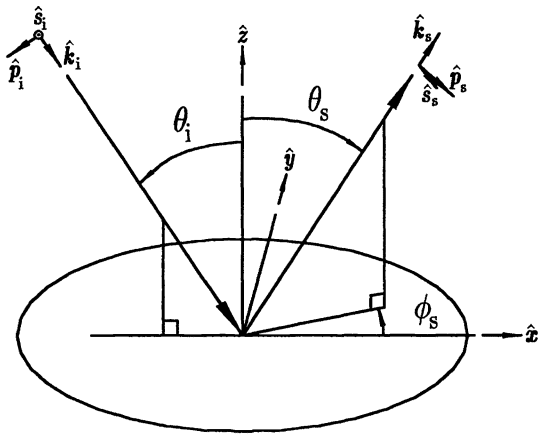

Figure 1 The sample coordinate system.

for light scattering from rough interfaces in a layered system. While the model fails to reproduce the data, some of the key aspects of the model are reproduced. The use of a pseudorandom two-level interface, however, does not constitute a sufficiently random rough interface for a model that does not include the effects of multiple scattering.

In Sec. 2, we will review the theoretical treatment for scattering from interfacial roughness. In Sec. 3, we will describe the experimental procedure employed for these measurements. In Sec. 4, we will present and discuss the results. Finally, the results will be summarized in Sec. 5.

2. THEORY

Figure 1 shows the measurement geometry used for this study. Plane wave polarized light of wavelength λ irradiates the surface at an incident angle of θ_i in the plane defined by $\hat{x}$ and $\hat{z}$. We are interested in calculating the Jones or Mueller matrix for scattering into a direction defined by a polar angle θ_s and an out-of-plane angle ϕ_s. Unit vectors $\hat{k}_i$ and $\hat{k}_s$ describe the directions of propagation of the incident and scattered light, respectively. The polarization of the incident field is described by the components of the electric field along the $\hat{s}_i$ and $\hat{p}_i$ directions, where $\hat{s}_i$ is a unit vector perpendicular to both $\hat{k}_i$ and $\hat{z}$, and $\hat{p}_i = \hat{k}_i \times \hat{s}_i$. Likewise, the polarization of the scattered field in a particular direction is described by the components of the electric field along the $\hat{s}_s$ and $\hat{p}_s$ unit vectors, defined in an analogous manner as $\hat{s}_i$, $\hat{p}_i$, and $\hat{k}_i$. We say that incident light is p-polarized (s-polarized) when it is linearly polarized with its electric field in the $\hat{p}_i$ ($\hat{s}_i$) direction.

The scattering Jones matrix J is defined as the relationship between the incident and scattered fields:

$$\begin{pmatrix} E_p^{\text{scat}} \\ E_s^{\text{scat}} \end{pmatrix} = \frac{\exp(ikR)}{R} \begin{pmatrix} j_{pp} & j_{sp} \\ j_{ps} & j_{ss} \end{pmatrix} \begin{pmatrix} E_p^{\text{inc}} \\ E_s^{\text{inc}} \end{pmatrix}, \tag{1}$$

where R is the distance from the scatterer to the detector, and $k = 2\pi/\lambda$. The matrix J can also be represented in its Mueller matrix form, $M = \mathcal{M}(J)$, where the operator $\mathcal{M}$ is given by numerous texts.[6,7]

In this paper, we are concerned with the polarization of light scattered by a sample illustrated in Fig. 2. Elson described the solution to the first-order vector perturbation theory for scattering from interfacial microroughness in a dielectric stack.[8–12] Germer outlined the technique for converting this solution to a Mueller matrix for a given correlation between the different layers.[5]

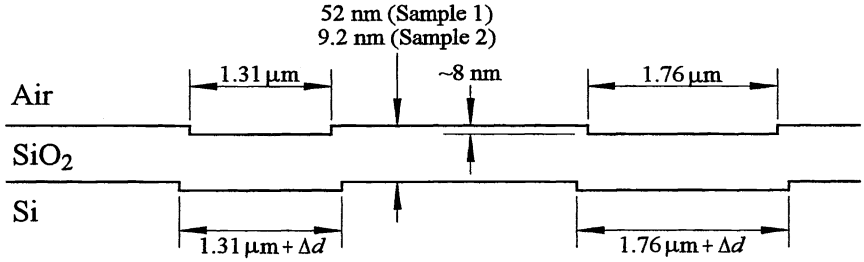

Figure 2 A diagram illustrating the characteristics of the samples studied. The vertical scale is not the same as the horizontal scale. The circular pits are pseudorandomly distributed about the wafer. The diameters of the lower pits may be different than their counterparts by Δd.

One of the powerful findings of the single interface studies was that the scattering matrix was a product of the power spectral density (PSD) function of the surface height and a polarization matrix, the latter depending only upon the incident direction, scattering direction, and the optical constants of the substrate.[3] Elson's theory leads to a similar result when two interfaces exist. The polarization matrix is then a function of the additional parameters of the optical constants of the overlayer, the thickness of the overlayer, the degree of correlation between the interfaces, and the relative amplitudes of the interfacial roughness.

The amplitude of the scattered field is proportional the Fourier transform $\Delta Z_n(\boldsymbol{k})$ of the roughness of the n-th interface, given by

$$\Delta Z_n(\hat{\boldsymbol{k}}_{ixy} - \hat{\boldsymbol{k}}_{sxy}) = (1/A)^{1/2} \int_A \mathrm{d}^2\boldsymbol{r}\ \Delta z_n(\boldsymbol{r})\ \exp[\mathrm{i}(\hat{\boldsymbol{k}}_{ixy} - \hat{\boldsymbol{k}}_{sxy}) \cdot \boldsymbol{r}], \tag{2}$$

where $\Delta z_n(\boldsymbol{r})$ is the surface height function of the n-th layer about its mean value, and the integration is carried out over the irradiated area A. The vectors $\hat{\boldsymbol{k}}_{ixy}$ and $\hat{\boldsymbol{k}}_{sxy}$ are the projections of $\hat{\boldsymbol{k}}_{\mathrm{i}}$ and $\hat{\boldsymbol{k}}_{\mathrm{s}}$ onto the xy plane, respectively, and are related to the scattering directions by

$$\begin{aligned} (\hat{\boldsymbol{k}}_{ixy} - \hat{\boldsymbol{k}}_{sxy})_x &= k(\sin\theta_{\mathrm{s}} \cos\phi_{\mathrm{s}} - \sin\theta_{\mathrm{i}}) \\ (\hat{\boldsymbol{k}}_{ixy} - \hat{\boldsymbol{k}}_{sxy})_y &= k(\sin\theta_{\mathrm{s}} \sin\phi_{\mathrm{s}}), \end{aligned} \tag{3}$$

where $()_\alpha$ denotes the α component of a vector. The Fourier transform of a cylindrical pit having depth a and diameter d is given by

$$\Delta Z(\boldsymbol{k}) = (1/A)^{1/2}(\pi a d/k) J_1(|\boldsymbol{k}|d/2), \tag{4}$$

where $J_1(x)$ is a first-order Bessel function. If the two interfaces are identical, then $\Delta Z_1(\boldsymbol{k}) = \Delta Z_2(\boldsymbol{k})$, and the polarization does not depend upon the $\Delta Z_n(\boldsymbol{k})$. In that case, the correlation coefficient is unity and the amplitudes of the two power spectra are the same. Note that there is no phase uncertainty in Eq. (4); the phases associated with different spatial frequencies are not random. If the bottom interface has pits of diameter $d + \Delta d$, due to undercutting from the isotropic growth of the layer (see Fig. 2), then the ratio of the Fourier transforms is given by

$$\Delta Z_2(\boldsymbol{k})/\Delta Z_1(\boldsymbol{k}) = [d/(d + \Delta d)] J_1(|\boldsymbol{k}|d/2)/J_1[|\boldsymbol{k}|(d + \Delta d)/2]. \tag{5}$$

Again, the absolute phase relationship is maintained, but the relative amplitude from each interface varies with spatial frequency.

In this paper, we are only concerned with the scattering from the two interfaces surrounding an SiO_2 layer on silicon. The modeling results shown in this paper assume that the index of refraction of the oxide is 1.46 at all the wavelengths studied.[13] The complex indices of refraction of silicon are assumed to be $3.882 + 0.019\mathrm{i}$ at 633 nm, $4.050 + 0.050\mathrm{i}$ at 532 nm, and $4.753 + 0.163\mathrm{i}$ at 442 nm.[13]

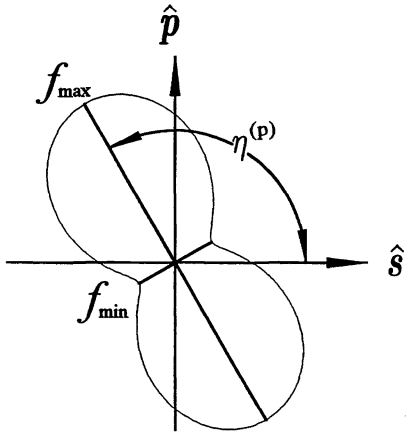

Figure 3 A schematic of the intensity distribution measured by a rotating linear polarization sensitive detector, defining the bidirectional ellipsometry parameters, $\eta^{(p)}$ and $P_L^{(p)} = (f_{max} - f_{min})/(f_{max} + f_{min})$.

3. EXPERIMENTAL DETAILS

The Goniometric Optical Scatter Instrument (GOSI), which was used to perform the measurements described in this paper, is described elsewhere.[14,15] Briefly, laser light of wavelength λ (λ = 633 nm, 532 nm, or 442 nm) is incident onto a sample at an angle θ_i, and light scattered into the direction defined by the angles $\{\theta_s, \phi_s\}$ is collected. The polarization state of the incident light is selected with a fixed linear polarizer followed by a rotating $\lambda/2$ linear retarder. The polarization state of the scattered light is analyzed with a rotating $\lambda/2$ linear retarder followed by a fixed linear polarizer. Although a bidirectional ellipsometric measurement can be carried out by fixing the incident light polarization while rotating the detection polarization optics, all of the measurements described in this paper were made by measuring the 3 × 3 non-handed Mueller matrix using a $(\omega, 4\omega)$ scheme,[16] whereby the receiving retarder is rotated at four times the rate of the incident light retarder. The signal is measured at 16 evenly spaced intervals, and the 9 elements of the 3 × 3 non-handed Mueller matrix are determined from the Fourier transform of those signals.

Figure 3 illustrates the definition of the bidirectional ellipsometry parameters. The angle $\eta^{(p)}$ is the angle that the principle axis of the polarization ellipse makes with respect to the $\hat{s}$ direction when p-polarized light is incident on the sample, and the degree of linear polarization $P_L^{(p)}$ is given by

$$P_L^{(p)} = (f_{max} - f_{min})/(f_{max} + f_{min}). \tag{6}$$

These parameters are easily derived from the non-handed Mueller matrix.[2] For linearly polarized light, $P_L^{(p)} = 1$, and for unpolarized light or circularly polarized light, $P_L^{(p)} = 0$.

For all of the measurements reported in this paper, the incident angle θ_i and the scattering angle θ_s were held fixed, while the azimuthal scattering angle ϕ_s was varied so that the polarization of scattered light into a cone was mapped out, and all but the extremes of the domain correspond to scattering out of the plane of incidence. When $\theta_i = \theta_s$, the magnitude of the spatial frequency of the roughness accessed by the measurement can be found from Eq. (3) to be given by $|\boldsymbol{k}| = 2\sin(\theta_s)\sin(\phi_s/2)/\lambda$.

The polarization properties of the scattered light from two samples were measured in this study. Both samples were microfabricated silicon microroughness standards with a pseudorandom distribution of two circular pits having nominal diameters of 1.31 μm and 1.76 μm and depths of approximately 8 nm, with one pit of each

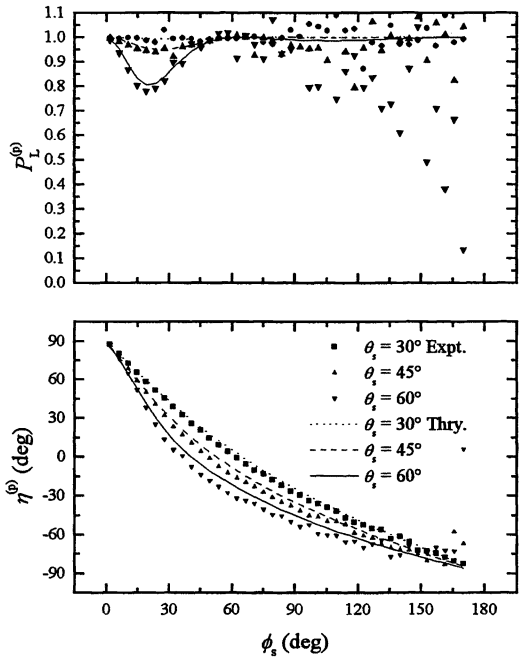

Figure 4 Bidirectional ellipsometry parameters, $P_L^{(p)}$ and $\eta^{(p)}$, for the 52 nm oxide sample as functions of azimuthal scattering angle, ϕ_s, for scattering angle $\theta_s = 30°$, 45°, and 60°. The wavelength was $\lambda = 633$ nm, and the incident angle was $\theta_i = 60°$. The symbols represent the measured data, and the curves represent the theoretical model for the case of correlated roughness.

diameter for every square on a 5 μm × 5 μm grid.[17] On each sample, an oxide layer was thermally grown, with thicknesses of 9.2 nm and 52 nm, respectively, as determined by spectroscopic ellipsometry on witness smooth samples. The roughnesses of the two interfaces on each sample are expected to be coherent, at least for long surface wavelengths (small $\boldsymbol{k}$). A side view schematic of the sample is shown in Fig. 2.

The random measurement uncertainties associated with $\eta^{(p)}$ and $P_L^{(p)}$ are estimated by Monte Carlo sampling over a Gaussian distribution about each measured mean value in the $(\omega, 4\omega)$ scheme with a width given by the respective measured standard deviation. The uncertainties shown with the data represent the standard deviation of the resulting distributions for $\eta^{(p)}$ and $P_L^{(p)}$. Other systematic sources of uncertainty may exist but are not expected to exceed 2° and 0.05 for $\eta^{(p)}$ and $P_L^{(p)}$, respectively, for most of the range of data. For ϕ_s near 115°, an artifact exists which can be attributed to scatter of the specular beam off the wall of the laboratory interfering with the small amount of scatter from the sample.

4. RESULTS AND DISCUSSION

Non-handed Mueller matrix measurements were carried out on the two samples for $\theta_i = 30°$, 45°, and 60°, for $\theta_s = 30°$, 45°, and 60°, and for $\lambda = 633$ nm, 532 nm, and 442 nm. A further set of measurements was carried out in the $\theta_i = \theta_s = 60°$ geometry at nine different locations on the wafer. In order to substantially reduce the amount of data shown, we display only the bidirectional ellipsometry parameters for p-polarized incident light. Figure 4 shows these parameters for $\theta_i = 60°$ and $\lambda = 633$ nm for the sample with a 52 nm thick overlayer.

The predictions of the model for correlated roughness are shown as curves in Figure 4. The model predicts a dip in $P_L^{(p)}$ near $\phi_s = 20°$. The existence, the magnitude, and the location of this dip are relatively well predicted

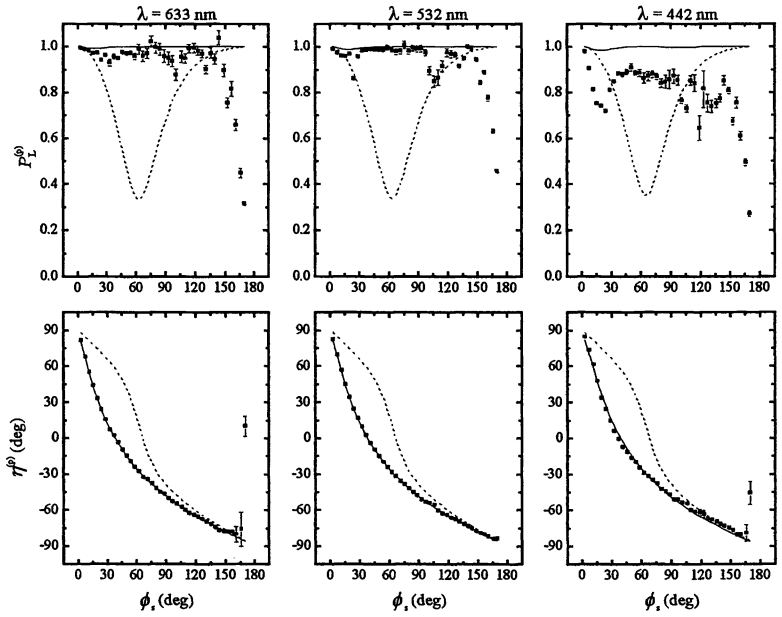

Figure 5 Bidirectional ellipsometry parameters, $P_{\mathrm{L}}^{(\mathrm{p})}$ and $\eta^{(\mathrm{p})}$, as functions of azimuthal scattering angle, ϕ_{s}, for the 9.2 nm oxide sample and for $\lambda = 633$ nm, 532 nm, and 442 nm. The angles $\theta_{\mathrm{i}} = \theta_{\mathrm{s}} = 60°$. The symbols represent the measured data, and the curves represent the theoretical model in the two limiting cases of correlated (solid) and uncorrelated (dashed) roughness.

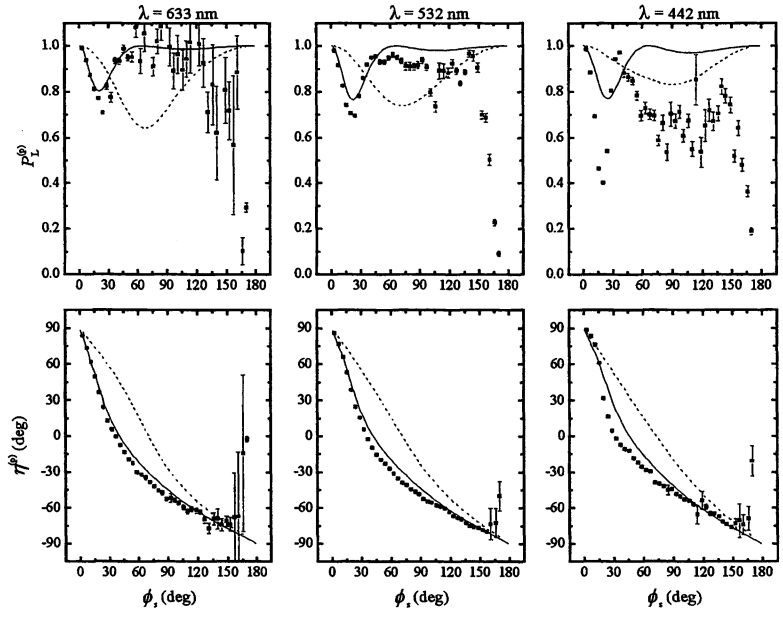

Figure 6 Same as Fig. 5, except for the 52 nm oxide sample.

by the model at 633 nm. That the theory predicts $P_L^{(p)} < 1$ indicates that the scattered light has a degree of elliptical polarization. The agreement between theory and experiment for $\eta^{(p)}$ is fine for $\phi_s < 15°$, but becomes poorer beyond this angle.

Figures 5 and 6 summarize the results of the bidirectional ellipsometry parameters for the two samples and the three wavelengths for the $\theta_i = \theta_s = 60°$ geometry. Shown in the figures are the predictions of the model for both correlated and uncorrelated roughness. The correlated roughness model and the data, as was shown in Fig. 4, agrees reasonably well at 633 nm for $P_L^{(p)}$. However, the agreement becomes progressively worse as the wavelength is decreased. The theory predicts that the magnitude of the dip in $P_L^{(p)}$ near 20° should remain nearly constant in amplitude. The data, however, shows a marked increase in the size of this dip. Similarly, the agreement between theory and experiment for $\eta^{(p)}$ becomes poorer as the wavelength is decreased.

The model parameters (indices of refraction, film thickness, correlation coefficient, relative roughness amplitude, and relative phase) were varied in an attempt to improve the agreement between theory and experiment. However, no set of parameters could be found that would fit the data in a consistent manner. It was possible to adjust the parameters in order to fit the data at one wavelength. However, these parameters were non-physical and did not agree with those determined at other wavelengths.

By comparing the second-order diffraction intensity to the first-order diffraction intensity for a sinusoidal surface, Vorburger *et al.* estimated that for rms surface roughnesses less than $\lambda/20$, first order vector perturbation theory should model the scattering properties well.[18] The samples studied here have a rms roughness of approximately 1.9 nm over the bandwidth 0.05 μm^{-1} to 12.6 μm^{-1} (determined by atomic force microscopy), which would be well within this limit. In fact, for scattering from a similarly-produced single interface, without the presence of the overlayer, the polarization indeed follows the predictions of the theory very well.[2] However, locally, the roughness is much larger than that indicated by the rms roughness. The actual peak-to-peak size of the roughness is approximately 8 nm, a value which is much closer to the prescribed limits of the model for $\lambda = 442$ nm ($\lambda/20 = 22$ nm). Although in the far field it is difficult to separate scattering which occurs from plateaus from that which occurs from edges (since without one, there cannot exist the other), in the near field, the fields are mostly distorted from plane waves in the vicinity of the edges. With the overlayer, each edge lies in close proximity to another edge as well as to the image of itself in the other interface. Therefore, one would expect a much higher degree of interaction between the edges than that predicted by first order perturbation theory. That one expects this breakdown in the model to occur at shorter wavelengths is consistent with the data.

To test these conclusions, bidirectional ellipsometry measurements from oxide films grown on silicon having significantly shallower pits can be made. In this case, the scattering would be expected to be substantially smaller, reducing the effects of edge-edge interactions or multiple scattering. Results from such measurements, together with modeling of edge-edge interactions, will be presented in the future.

The effects of undercutting are illustrated with model calculations in Fig. 7. In these calculations, two pits, of nominal diameters $d_1 = 1.31$ μm and $d_2 = 1.76$ μm, are assumed to be undercut by 5 nm after growth of a 52 nm film. The two different sized pits are uncorrelated with respect to each other, so that their respective signals are added as Mueller matrices. One observes deviations from that expected for the non-undercut pits near $\phi_s = 50°$ and $\phi_s = 75°$ for 442 nm. These deviations can be observed in the 442 nm $\eta^{(p)}$ data in Fig. 6 near these same angles. It is not expected that multiple scattering would strongly affect the location of these features, since they are determined by conservation of momentum considerations. Multiple scattering may, however, modify their amplitudes or widths. Since the rest of the data is rather poorly fit by the model, we will not attempt to extract quantitative information from these features. However, the technique of polarized light scattering may prove to be useful for evaluating such dimensional changes upon film growth once the models are improved.

Although we did not measure the circular components of the polarization, the relative lack of positional dependence to $P_L^{(p)}$ suggests that, at least for the small scattering angles near the dip in $P_L^{(p)}$, the scattered light

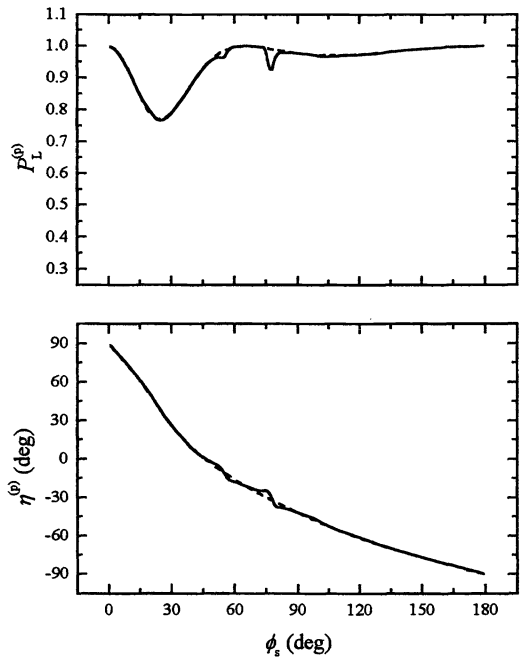

Figure 7 Calculated effect of undercutting on the bidirectional ellipsometry parameters, $P_L^{(p)}$ and $\eta^{(p)}$, for the 52 nm oxide sample as functions of azimuthal scattering angle, ϕ_s, for $\lambda = 442$ nm and $\theta_i = \theta_s = 60°$. The solid curve shows the effect of a radius reduction of 5 nm on the lower interface. The dashed curve shows the calculation without undercutting. Both surfaces are assumed to be otherwise correlated.

is still highly polarized. This behavior is required in order to fully exploit the ability to make a microroughness-blind scattering instrument. Indeed, if that is the case, then one can make a microroughness-blind instrument which will not "see" the scatter from the rough interfaces on these samples. However, since the samples do not behave like real pairs of random rough interfaces, such samples would not be particularly useful for the alignment of such an instrument, since the properties of a natural surface is expected to scatter differently.

The development of an artifact standard that behaves like a true rough surface with a dielectric layer would allow instruments to calibrate their sensitivity to roughness in the presence of dielectric layers. The photolithographically generated microrough surface without the dielectric layer was shown in previous measurements[2,3] to behave very much like a random rough surface, in that the polarization of the light scattered replicated that of a true random rough surface. If an artifact were intended to mimic natural roughness with a dielectric layer, it must also reproduce the polarization behavior as well as the intensity. Since the scattering from these samples does not replicate the scatter from a truly random rough surface with a correlated dielectric layer, then the application of these samples as reference scatterers is at risk.

5. SUMMARY

Measurements were made of the polarization of light scattered by 9.2 nm and 52 nm films grown on photolithographically produced microrough silicon. First order vector perturbation theory failed to reproduce the experimental results. The lack of agreement is attributed to the breakdown of the model, which ignores interactions between features on two different interfaces. These interactions are expected to be much stronger on the artificially produced rough interfaces compared to those for naturally rough interfaces.

ACKNOWLEDGEMENTS

The authors would like to thank Dr. Fei Xu for performing atomic force measurements of the samples.

REFERENCES

[1] T. A. Germer, "Angular dependence and polarization of out-of-plane optical scattering from particulate contamination, subsurface defects, and surface microroughness," Appl. Opt. **36**, 8798–805 (1997).

[2] T. A. Germer, and C. C. Asmail, "Bidirectional ellipsometry and its application to the characterization of surfaces," in *Polarization: Measurement, Analysis, and Remote Sensing*, D. H. Goldstein, and R. A. Chipman, ed., Proc. SPIE **3121**, 173–82 (1997).

[3] T. A. Germer, C. C. Asmail, and B. W. Scheer, "Polarization of out-of-plane scattering from microrough silicon," Opt. Lett. **22**, 1284–6 (1997).

[4] T. A. Germer, and C. C. Asmail, "Microroughness-blind hemispherical optical scatter instrument," U.S. Patent Application filed (1998).

[5] T. A. Germer, "Application of bidirectional ellipsometry to the characterization of roughness and defects in dielectric layers," in *Flatness, Roughness, and Discrete Defect Characterization for Computer Disks, Wafers, and Flat Panel Displays II*, J. C. Stover, ed., Proc. SPIE **3275**, 121–31 (1998).

[6] H. C. v. d. Hulst, *Light Scattering by Small Particles*, (Dover, New York, 1981).

[7] C. F. Bohren, and D. R. Huffman, *Absorption and Scattering of Light by Small Particles*, (Wiley, New York, 1983).

[8] J. M. Elson, "Multilayer-coated optics: guided-wave coupling and scattering by means of interface random roughness," J. Opt. Soc. Am. A **12**, 729–42 (1995).

[9] J. M. Elson, J. P. Rahn, and J. M. Bennett, "Light scattering from multilayer optics: comparison of theory and experiment," Appl. Opt. **19**, 669–79 (1980).

[10] J. M. Elson, "Diffraction and diffuse scattering from dielectric multilayers," J. Opt. Soc. Am. **69**, 48–54 (1979).

[11] J. M. Elson, "Infrared light scattering from surfaces covered with multiple dielectric overlayers," Appl. Opt. **16**, 2873–81 (1977).

[12] J. M. Elson, "Light scattering from surfaces with a single dielectric overlayer," J. Opt. Soc. Am. **66**, 682–94 (1976).

[13] E. D. Palik, *Handbook of Optical Constants of Solids*, (Academic, San Diego, 1985).

[14] C. C. Asmail, C. L. Cromer, J. E. Proctor, and J. J. Hsia, "Instrumentation at the National Institute of Standards and Technology for bidirectional reflectance distribution function (BRDF) measurements," in *Stray Radiation in Optical Systems III*, R. P. Breault, ed., Proc. SPIE **2260**, 52–61 (1994).

[15] T. A. Germer, and C. C. Asmail, "A goniometric optical scatter instrument for bidirectional reflectance distribution function measurements with out -of-plane and polarimetry capabilities," in *Scattering and Surface Roughness*, Z.-H. Gu, and A. A. Maradudin, ed., Proc. SPIE **3141**, 220–31 (1997).

[16] R. M. A. Azzam, "Photopolarimetric measurement of the Mueller matrix by Fourier analysis of a single detected signal," Opt. Lett. **2**, 148 (1978).

[17] B. W. Scheer, "Development of a physical haze and microroughness standard," in *Flatness, Roughness, and Discrete Defect Characterization for Computer Disks, Wafers, and Flat Panel Displays*, J. C. Stover, ed., Proc. SPIE **2862**, 78–95 (1996).

[18] T. V. Vorburger, E. Marx, and T. R. Lettieri, "Regimes of surface roughness measurable with light scattering," Appl. Opt. **32**, 3401-8 (1993).